The Application of Tactile, Audible, and Ultrasonic Forces to Human Fingertips Using Broadband Electroadhesion

Craig Shultz, *Member, IEEE*, Michael Peshkin, *Senior Member, IEEE*, and J. Edward Colgate, *Fellow, IEEE*

Abstract—We report an electroadhesive approach to controlling friction forces on sliding fingertips which is capable of producing vibrations across an exceedingly broad range of tactile, audible, and ultrasonic frequencies. Vibrations on the skin can be felt directly, and vibrations in the air can be heard emanating from the finger. Additionally, we report evidence from an investigation of the electrical dynamics of the system suggesting that an air gap at the skin/surface interface is primarily responsible for the induced electrostatic attraction underlying the electroadhesion effect. We developed an experimental apparatus capable of recording friction forces up to a frequency of 6 kHz, and used it to characterize two different electroadhesive systems, both of which exhibit flat force magnitude responses throughout the measurement range. These systems use custom electrical hardware to modulate a high frequency current and apply surprisingly low distortion, broadband forces to the skin. Recordings of skin vibrations with a laser Doppler vibrometer demonstrate the tactile capabilities of the system, while recordings of vibrations in the air with a MEMS microphone quantify the audible response and reveal the existence of ultrasonic forces applied to the skin via electronic friction modulation. Implications for surface haptic and audio-haptic displays are briefly discussed.

Index Terms—Surface haptics, electroadhesion, electrovibration, haptic display, audio-tactile display

1 Introduction

Surface haptic displays aim to apply programmable forces to bare fingertips on flat surfaces. Geared towards enriching the user experience of touchscreen devices, these displays show promise of being seamlessly incorporated into everyday human computer interactions. One class of surface haptic device that has received great interest is the variable friction display.

When operated at steady state, variable friction displays are able to arrest the motion of a sliding finger, or reduce friction to a near negligible level. These effects are achieved by applying additional electrostatic force, which increases friction [1], [2], [3], or by altering the skin/surface interface via low amplitude, ultrasonic oscillations [4], [5], which decreases friction. These effects can also be combined for greater dynamic range [6].

1.1 Quasi-Static versus Dynamic Actuation

While the quasi-static behavior of these displays has been the primary subject of research for some time by our lab and others, more recent applications utilize increasingly rapid modulation of friction. This transition towards dynamic actuation stems from the fact that all known variable friction displays (including those presented here) actuate the entire fingerpad in spatial synchrony, i.e., the entire fingerpad is altered at once. This synchrony offers impoverished information to slowly adapting type I tactile afferents (Merkel's discs), which are sensitive to quasi-static (< 10 Hz) spatial distributions of strain energy across the fingerpad. In contrast, dynamic modulation of friction (> 10 Hz) is thought to offer rich information for both fast adapting type I (Messiner's Corpuscles) and type II (Pacinian Corpuscles) tactile afferents, which are most sensitive to transient and broadband vibrations in the range of approximately 10-1,000 Hz, and which can have less spatial acuity [7], [8]. The fast adapting afferents, therefore, appear to be prime candidates for spatially synchronous variable friction actuation. In fact, properly actuating the fingertip at these dynamic frequencies (10-1,000 Hz) may be critical to new surface haptic applications such as virtual texture display [9], [10].

1.2 Example Application: Surface Texture

Variable friction displays appear particularly well suited for the display of virtual surface texture. In this context, the interaction forces encountered by a finger sliding on real texture can be modeled by a slowly varying friction component that changes over a coarse spatial period, representing localized features, and a rapidly oscillating friction component, representing fine textural features [10].

These interaction forces cause vibrations in the finger that are broadband in nature, particularly for fine surface textures, containing appreciable power in the hundreds of Hertz range [11]. These vibrations trigger strong tactile afferent

• *The authors are with the Department of Mechanical Engineering, Northwestern University, Chicago, IL 60208. E-mail: craigdshultz@u.northwestern.edu, {peshkin, colgate}@northwestern.edu.*

Manuscript received 2 Oct. 2017; revised 15 Dec. 2017; accepted 26 Dec. 2017. Date of publication 15 Jan. 2018; date of current version 15 June 2018. (Corresponding author: Craig Shultz.) Recommended for acceptance by F. Giraud. For information on obtaining reprints of this article, please send e-mail to: reprints@ieee.org, and reference the Digital Object Identifier below. Digital Object Identifier no. 10.1109/TOH.2018.2793867

responses, particularly in fast adapting afferents, which capture the spectral content of these vibrations with millisecond spike timing precision [12]. Furthermore, this precise timing appears to be preserved in the firing of somatosensory cortex neurons (primarily derived from fast adapting type II afferents) and also appears to influence tactile perception [13].

It seems then that a consistent approach to virtual surface texture display could be to faithfully reproduce these same patterns of interaction force that have been measured with real world textures with the aim of achieving the same vibrations, cortical firing patterns, and, ultimately, tactile perception of surface texture.

A principal goal of this research, therefore, is to develop an approach to variable friction surface haptics that is sufficiently broadband to offer rich excitation of fast adapting type I and II afferents. Additionally, this approach should have an ideally flat dynamic force response in the range of 10-1,000 Hz. In this paper we demonstrate that not only is this broadband tactile excitation possible, but the method and hardware developed may be easily extended to produce programmable audio emanating from a fingertip, adding a complementary sensory modality to the interaction experience. As a side-effect of the modulation method, it is also shown that ultrasonic friction forces (up to at least 50-60 kHz) can also be applied to the finger. These results indicate that the only major limitation to the bandwidth of the electroadhesion effect appears to be the speed at which the electric field may be applied to the system.

2 Background

2.1 Wide-Bandwidth Variable Friction

The quasi-static behavior of variable friction devices has been previously addressed in the literature and will be briefly addressed in this work. An emergent area of study, however, is devoted to the question of system dynamic response.

In 2014, Meyer et al. [14] performed initial bandwidth measurements on electroadhesive and ultrasonic variable friction devices, showing overall magnitude and transient responses. Both methods exhibited roll-offs in force starting around 130 Hz. Beyond this frequency, the ultrasonic device continued to show additional force attenuation, while the electroadhesive device appeared to flatten out to until the end of their 1 kHz measurement range. The authors proposed a second-order resonant mechanical model to partially explain the attenuation of the ultrasonic device, but offered limited characterization of the electroadhesive device. They only suggested that electroadhesive devices are more responsive than their ultrasonic counterparts, presumably due to their solid state nature. A conclusion was that electroadhesive surfaces showed promise for wide-bandwidth force display.

Followup work showed that the limited bandwidth of the ultrasonic device could be mostly corrected for by using a compensation filter and high performance piezo amplifier, capable of driving the piezos at an increasing voltage with increasing modulation frequency [15]. These techniques led to improved high frequency performance at the cost of added complexity and power consumption. This inherent tradeoff between bandwidth and power consumption in ultrasonic devices was also commented on by Wiertlewski et al. [16].

Similar transient step response measurements were made on ultrasonic and electroadhesive devices by Vezzoli et al. [6]. Their measurements supported the conclusion that ultrasonic devices are limited by resonance. They also hypothesized that electroadhesive devices should only be limited by amplifier bandwidth, and that a high-bandwidth amplifier should yield high-bandwidth forces. This work employs such an amplifier, and details the manner of its application.

2.2 Electroadhesion: A Physical Phenomenon

The term electroadhesion refers to the generalized physical principle of increased adhesion between two contacting surfaces brought about by the application of electrostatic attraction across their interface [17]. While the name is drawn from the work of early 20th century scientists studying the effect [3], the earliest known observations of electroadhesion occurred in the late 1800s, predating, and in fact precipitating, the controversial invention of the telephone in 1876 [18]. Discovered in 1874 and detailed in a patent in 1875 by American inventor Elisha Gray, the acoustic vibration induced by an electric current flowing through a finger sliding on a conductive acoustic body was used as an early example of how an electrical telegraph could be utilized to convey musical tones across a wire [19].

Gray's method of transduction, however, was usurped by more practical designs and it was seemingly neglected until its rediscovery, once again because of sliding fingers, by the Danish scientists Johnsen and Rahbek in the early 1920s [17]. Forgotten yet again, it was rediscovered and documented in the 1950s by Mallinckrodt running his finger across a poorly wired light socket [20].

The effect was first used for tactile display purposes in 1970 [21], and a subset of the effect garnered the name electrovibration in 1983 [22]. A later electrotactile display was made by Beebe et al. [23], and the first applications of the effect for visuo-tactile display were described by Linjama and Mäkinen [1], followed by Bau et al. [2]. The first systematic force measurements with human fingers were made by Meyer et al. [24]. This work was also the first known attempt to introduce high frequency amplitude modulation to generate a constant adhesion force that could be adjusted arbitrarily. This method of actuation differed from previous so-called electrovibration devices which utilized electroadhesive force ripple, typically produced by applying single frequency voltage excitation to the finger.

All modern devices, however, still only produced force on the finger via polarized bound charge. In contrast, Shultz et al. [3] described and demonstrated the first modern usage of free charge to produce force, an effect sometimes named after Johnsen and Rahbek. This work also introduced an electrical impedance based force model to unite bound and free charge effects, and, in doing so, suggested electroadhesion as a general term to encompass all manners of electrostatic attraction based devices (a convention adopted here).

3 Methods and Apparatus

3.1 Rotational Tribometer

A custom rotational tribometer was constructed to provide a velocity and normal force controlled platform for various experiments. The rotational nature of the device allows repeatable data capture of long time records (10-100 s) and ensures good control of velocity, with no abrupt changes in velocity direction. The device was built around a modified

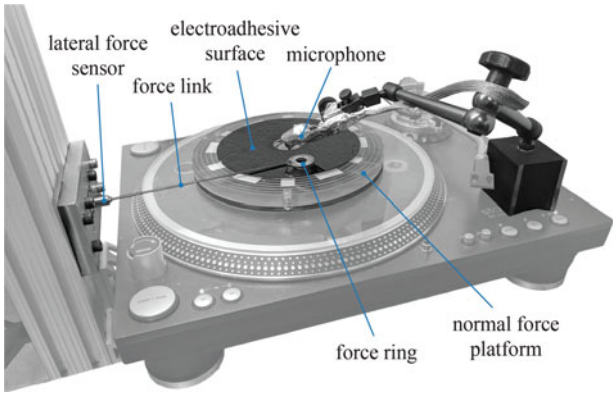

Fig. 1. Overview of rotational tribometer apparatus and recording instruments. The rotational slip ring, hand rest, and supporting frame have been temporarily removed for clarity.

turntable (ST.150, Gibson Guitar Company, TN, USA). Data was collected using a 16 bit data acquisition (DAQ) board (NI USB-6361, National Instruments, TX, USA) with a sampling rate of 250 kHz. The direct drive turntable maintains a constant rotational velocity via an internal controller, and is monitored by reading the internal quadrature encoder. The translational velocity at the finger was held at 170 mm/s for all experiments, accomplished by setting the turntable to a prescribed rotational velocity, and keeping the finger a set distance from the center of rotation. A general layout of the apparatus can be seen in Fig. 1.

Normal force applied by the finger was monitored using a custom force platform based on three piezoresistive force sensors (FSS1500NSR, Honeywell, MN, USA) mounted to a 12 mm thick acrylic disc. The force signal was conveyed off of the platform using a rotational slip ring and displayed on a visual screen for user feedback. Normal force was held at 1N by the user (using this visual feedback) for all experiments.

Lateral force was measured using a piezoelectric force sensor and charge amplifier (9217A and 5010B, Kistler Instrumente AG, Winterthur, Switzerland) which was coupled to a patch of skin contacting the rotating plate via a carbon fiber link and a 0.5 mm thick FR4 fiberglass ring with 25 mm OD and 13 mm ID (also shown in Fig. 4a). A PTFE ring spacer, 0.5 mm thick with 25 mm OD and 23 mm ID, was affixed to the bottom of the fiberglass ring. This spacer ensures that any normal force not traveling though the contact patch has minimal effect on measured lateral force. It also constrains the apparent contact area of the skin to $\approx 100\,\mathrm{mm}^2$, allowing electrical measurements to be made with a well defined contact area.

3.2 Electroadhesive Surfaces

Two 150 mm diameter discs with electroadhesive surface coatings were used for experiments, as seen in Fig. 2. One is common to the literature, and one is relatively new. Both coatings were chosen primarily due to their electrical and frictional properties. In particular, each surface shows good stability in friction force with fingertip sweat pore occlusion, allowing friction measurements that are consistent over long time scales. Each surface also exhibits appreciable electroadhesive effects across an exceedingly wide range of frequencies and with relatively small applied voltages. This allows a wide variety of measurements to be made.

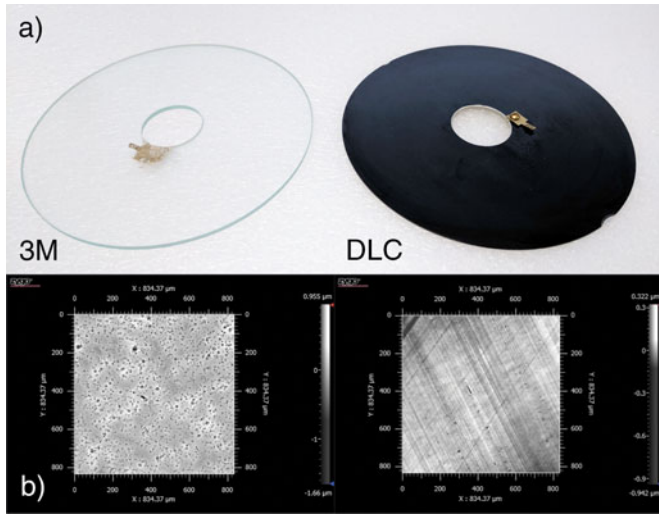

Fig. 2. a) Transparent 3M MicroTouch silica coated glass substrate (left), and mildly opaque black DLC BALINIT DYLYN PRO coated substrate (right). b) Optical profilometry image of an approximate 0.8x0.8 mm patch of 3M (left) and DLC (right) coatings.

The transparent disc on the left of Fig. 2 was cut from a readily available touch screen system sold by 3M (tradename 3M MicroTouch^{TM}). It's referred to here as the 3M coating. The disc consists of a 3 mm thick glass substrate, on top of which is a 40 nm indium tin oxide (ITO) conductive layer, and a 1 μm SiO_2 dielectric layer [24]. Notably, this surface coating was chosen as it has become increasingly popular with a number of research groups utilizing the electroadhesive effect [2], [24], [25], [26], [27], [28].

The disc was cut using a CNC waterjet cutter specifically adapted to cut glass. The cutting process exposes the edge of the conductive ITO layer, and a new direct electrical connection was made to this layer by applying conductive silver epoxy along the cut edge of the glass. This epoxy is then also bonded to a brass spade connector, which is used as the new electrical connection point. Importantly, this separate connection to the ITO layer bypasses the normal series capacitance of 3M MicroTouch screens which, if left in place, results in a substantial voltage attenuation in the system, necessitating the need for higher driving voltages. This series capacitance is also thought to dramatically impact the electrical dynamics of the system at low frequency, as modeled in [24]. This is believed to be the first reported work which removes this capacitance.

The second electroadhesive surface (seen on the right Fig. 2) used was a 1mm thick aluminum disc. This disc was coated with a diamond like carbon (DLC) coating using a chemical vapor deposition (CVD) process. It is referred to here as the DLC coating. It is approximatly 2 μm thick and goes by the trade-name BALINIT DYLYN PRO. This coating is specifically designed for plastic injection molding type applications, and has low surface adhesion characteristics. It was chosen to offer a comparison to the 3M coated surface, and to highlight the ubiquity of the broadband electroadhesive effect with thin, low friction surface coatings.

The topographic roughnesses of each surface, shown in Fig. 2b, was characterized by a 3D optical surface profiler (Nexview, Zygo Corporation, PA, USA). The 3M coating has and RMS roughness of 193 nm, while the DLC coating has an RMS roughness of 35 nm. Profilometery also

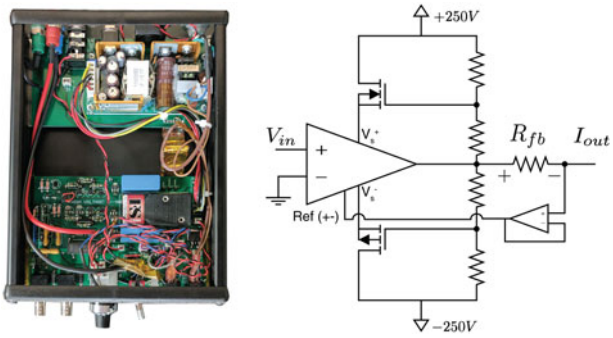

Fig. 3. High voltage compliant current controlled amplifier with integrated voltage and current sensing circuitry (left) and a simplified electrical schematic showing the amplifier operating principle (right).

revealed the abundance of microscopic pores on the surface of the 3 M coating that appear to partially, or perhaps fully, penetrate the silica layer. In contrast, the DLC coating appears to have good conformity, and no pinholes were observed.

3.3 High Performance Current Controller

Current control is utilized in all experiments for two primary and related reasons: safety and uniformity of effect. Recommended current threshold levels outlined in [29], [30] were adhered to for all experiments, and applied current remained below the limit of electrocutaneous stimulation.

An effective way to ensure this current threshold is with a current controlled source. A voltage controlled source is susceptible to sudden decreases in total system impedance (such as dielectric coating breakdown or sweat accumulation between the finger and surface) which can result in sudden increases in total system current beyond recommended thresholds (shorting). The insensitivity current control offers to changes in system impedance also implies increased uniformity in electroadhesive effect, as it imposes a more uniform voltage across the skin/surface interface regardless of changes in skin, surface, or other environmental impedances such as poor grounding conditions.

A custom high voltage compliant, transcondutance amplifier, seen in Fig. 3 (left), was constructed and characterized. The amplifier can source or sink up to 5 mA with a voltage compliance of ±250 V. It is built around a high common mode voltage differential amplifier (AD8479, Analog Devices Inc, MA, USA) and DC/DC converter (FS05CT-12, XP Power, CA, USA) in a bootstrapped power supply configuration [31]. Current is controlled via a 1 kΩ 0.1 percent feedback resistor in a modified Howland current source topology. A highly simplified schematic of this circuit topology can be seen in Fig. 3 (right). Input voltage V_{in} is applied across the input terminals of the differential amplifier. This amplifier then outputs a current, I_{out}, across R_{fb} such that the voltage across R_{fb} is the same as V_{in}. This is accomplished by buffering the output voltage, V_{out}, with a voltage follower and applying this signal to the Ref+ and Ref- terminals of the differential amplifier. The transconductance gain of this amplifier, therefore, is equal to $1/R_{fb} = 1$ mA/V. The resistor ladder and feedback transistors (PCH, VP2450N3-G, Microchip Technology, NCH, STQ1NK80ZR-AP, STMicroelectrics) perform the bootstrapping operation in the circuit, floating the differential amplifier power supplies above and below the required output voltage. See [31] for more details on the bootstrapping operation principles.

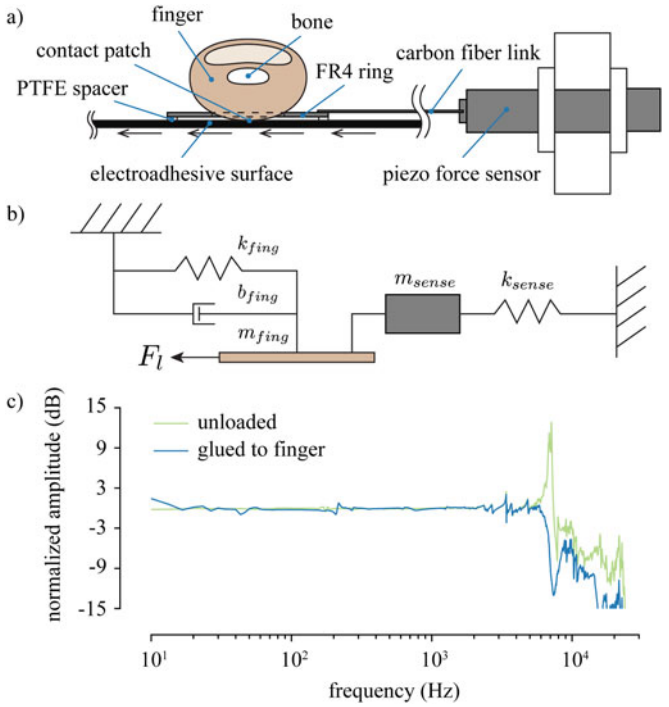

Fig. 4. a) Cross-section of a finger, glued to a FR4 ring, pressed against the rotating electroadhesive surface. The FR4 ring is affixed to a carbon fiber link and piezo force sensor. b) Lumped lateral impedance model showing the connection of the finger mass and force link/sensor. c) Normalized impulse response of a ball bearing pendulum striking the force link/sensor in axial compression.

Current was supplied to the rotating surface via an electrical slip ring. When the surface is touched, current travels through the surface coating and into skin of the finger. It then exits the body by way of a Ag/AgCl electrode applied to the user's wrist. Another 1 kΩ 0.1 percent shunt resistor was used to measure return current from the electrode, and a custom 50:1 high impedance (≈500M Ω||10pF) probe was used to measure total applied voltage.

An equivalent output impedance of the amplifier was measured to be on the order of 20 MΩ, limited only by the input common mode rejection ratio (CMRR) of the differential amplifier. The amplifier bandwidth is partially limited by stray output capacitance to ground, and a capacitance compensation positive feedback circuit was utilized to mitigate this effect. With capacitance compensation, the measured large signal -3 dB bandwidth into a typical RC load impedance was 45 kHz. Additionally, total harmonic distortion (THD) for applied current was measured to be less than 1 percent throughout this entire range. Redundant internal safety mechanisms limit the possible applied current to < 10 mA.

3.4 Lateral Force Sensing

A representation of the lateral force measurement setup can be seen in Fig. 4a. The FR4 ring is glued to the perimeter of the skin contact patch using cyanoacrylate adhesive prior to measurements. This ring is intended to isolate the contact patch from the rest of the finger and bone. When linked to the force sensor, it serves to shunt the contact patch lateral stiffness to the bone with the much higher stiffness of the sensor, while adding minimal moving mass (Fig. 4b).

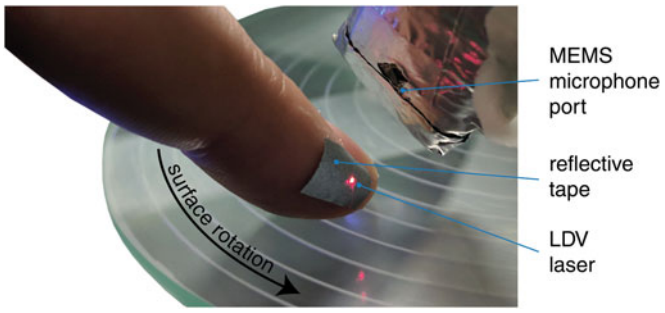

Fig. 5. Measurement setup for recording vibrations on the skin and in the air as a result of the electroadhesive friction force. Note: The finger is free only during the measurement of vibration (Fig. 10). For other measurements, it is glued to the force ring.

The low frequency lateral impedance of an engaged fingertip to bone can be modeled by a linear spring-mass-damper system, with a damped natural resonance occurring around 250 Hz [32]. The equivalent stiffness of a typical fingertip skin patch is low ($\approx$ 1 N/mm), as is the moving mass ($\approx$ 0.1 g). The piezo force sensor used has a stiffness four orders of magnitude greater ($\approx$ 15000 N/mm) and a small moving mass ($<$ 1 g). The carbon fiber link and fiberglass ring were designed to achieve a high stiffness to weight ratio, so as to reduce their impact on the sensor's performance. The distributed mass and stiffness are lumped into m_{sense} and k_{sense}.

Averaged impulse responses of the force link/sensor are shown in Fig. 4c. These responses show a large compression mode resonance at approximately 7 kHz, which is damped when the lead author's finger is glued to the force ring. This analysis implies that, below the resonance of the force link/sensor, the measured lateral force represents the applied lateral force at the perimeter of the skin contact patch.

3.5 Audible and Ultrasonic Microphone

Audio emanating from the fingertip was recorded using a MEMS microphone (SPU0410LR5H-QB, Knowles Electronics, IL, USA), seen in Figs. 1 and 5. This microphone's frequency response is flat from 100-10,000 Hz, exhibits a broad resonance at 20-30 kHz, and reduced but still appreciable sensitivity into the ultrasonic regime. This allows basic audio and ultrasonic vibration measurements to be made. The microphone was placed in the acoustic near field of the fingertip, as seen in Fig. 5.

3.6 Laser Doppler Vibrometer

Velocity of vibrations of the fingertip were recorded with a laser Doppler vibrometer (CLV-1000, Polytec GmbH, Waldbronn, Germany). The decoder range used supports a peak velocity of 250 mm/s at an accuracy of 1.5 um/s from 0.5 Hz to 250 kHz. The laser was focused onto a piece of retroreflective tape glued to the side of the lead author's non-dominant index finger, seen Fig. 5. The velocity measurement was approximately orthogonal to the fingertip and parallel to the direction of motion at the surface of the finger.

4 System Models

4.1 Fundamental Force Generation Model

The force model used here assumes that the relevant electroadhesive force serving to increase friction between the skin and surface acts not on the skin or surface coating in isolation, but rather across a small air gap formed at the interface of the two. It hypothesizes that this air gap can be modeled as a parallel plate capacitor which has a top plate defined by the outermost layer of stratum corneum and a bottom plate made by the top surface of the electroadhesive coating. With an electric field applied across this air gap, the magnitude of total additional electroadhesive normal force, F_e, pulling down on the charged surface of the skin can be written in scalar form as

$$|F_e| = |Q_{gap}| \frac{|E_{gap}|}{2}, \tag{1}$$

where Q_{gap} represents the total net charge on the outer surface of the stratum corneum, and E_{gap} represents the total electric field in the gap. Note the $1/2$ term comes from the fact that the charge in the stratum corneum feels only the force due to the electric field created by the opposing charge on the surface of the coating, which is half the total field. Equation (1) is a simplified statement of Coulomb's law for two parallel planes of opposite charge, and it lies at the heart of this electroadhesive force model. It implies that if charge is able to accumulate at edges of the air gap, (regardless of the charge being bound or free) and an electric field exists within that air gap, there should be an attractive force generated pulling the skin towards the surface coating and increasing friction. It can also be put into a more familiar form of a parallel plate capacitor with a distensible dielectric

$$F_e = \frac{A_{gap} \varepsilon_0 \varepsilon_{gap} V_{gap}^2}{2 d_{gap}^2}, \tag{2}$$

where A_{gap} is the effective air gap area, ε_0 is vacuum permittivity, ε_{gap} is the dielectric constant of the distensible gap ($\varepsilon_{gap} = 1$ for air), V_{gap} is the voltage between the two plates of charge, and d_{gap} is the plate separation.

4.2 Friction Model

The rotation of the turntable ensures a constant slip condition of the contact patch. No stick-slip behavior was observed, and if we model the lateral force conveyed during slipping using a Coulombic kinetic friction model, the effects of electroadhesion can be incorporated by including the additional component of normal force given by (2). This is represented below, where F_l is the lateral friction force (denoted in Fig. 4b), μ is the kinetic coefficient of friction, F_n is the externally applied normal force, and F_e is the instantaneously applied electroadhesive force.

$$F_l = \mu (F_n + F_e) \tag{3}$$

If F_n is held constant, and μ is assumed constant, then any additional lateral force, F_{add}, is solely proportional to additional applied electroadhesion force.

$$F_{add} = \mu F_e, \quad F_{add} = F_{lat} - \mu F_n \tag{4}$$

4.3 Electrical Impedance Model

A full electrical impedance characterization of the skin, 3M and DLC coatings, and the combined system was performed to validate the gap impedance electrical model introduced in [3]. This analysis is beyond the scope of this work, and we

report only on aspects of the model that inform the force measurements. This model states that the gap voltage described by (2) is related to the total applied current, I_{total}, via the complex air gap impedance, Z_{gap}, and Ohm's law

$$V_{gap} = I_{total} Z_{gap}. \tag{5}$$

Intuitively, the gap impedance can be thought of as the electrical impedance that remains from a measure of the total impedance after all other possible physical impedance mechanisms have been accounted for (such as the series impedances of the skin, body, bulk of the dielectric coating, etc.). It is the electrical impedance associated with the geometric and electrical contact conditions between the skin and surface during sliding.

It was found that this gap impedance accounted for approximately 80-90 percent of the total system impedance observed during sliding with the 3M coated surface, and between 60-80 percent with the DLC coated surface. This implies that, for these specific electroadhesive systems, the majority of the total applied voltage is dropped across the air gap impedance. Furthermore, it was found that the gap impedance exhibited two distinct operating regions, a low frequency resistive region and high frequency capacitive region, with a continuous transition zone between the regions from approximately 10 Hz to 1,000 Hz.

5 Impact of Gap Impedance on Force Bandwidth

5.1 Predicted Impact

Incorporating the series impedance based electrical model with our force equations, we can begin to predict the impact of the electrical dynamics of the air gap on the force transduction bandwidth. Combining Equations (2), (4), and (5) yields

$$F_{add} = \frac{\mu A_{gap} \varepsilon_0 \varepsilon_{gap}}{2 d_{gap}^2} (I_{total} Z_{gap})^2, \tag{6}$$

which is a general equation for the additional lateral force measured by the piezo force sensor given the applied total current and gap impedance. Note that, for this model and our experiments, only the total applied current and gap impedance are assumed to change much with time or frequency. With this assumption we can lump the other system parameters into a single scaling constant

$$\alpha = \frac{\mu A_{gap} \varepsilon_0 \varepsilon_{gap}}{2 d_{gap}^2}, \tag{7}$$

and therefore,

$$F_{add} = \alpha (I_{total} Z_{gap})^2. \tag{8}$$

This equation predicts two important points for current controlled electroadhesive excitation:

(1) The bandwidth of the current controller will directly impact the bandwidth of the electroadhesive force.
(2) For a constant amplitude current source, the resulting dynamic characteristic of the electroadhesive force will mimic that of the air gap impedance squared.

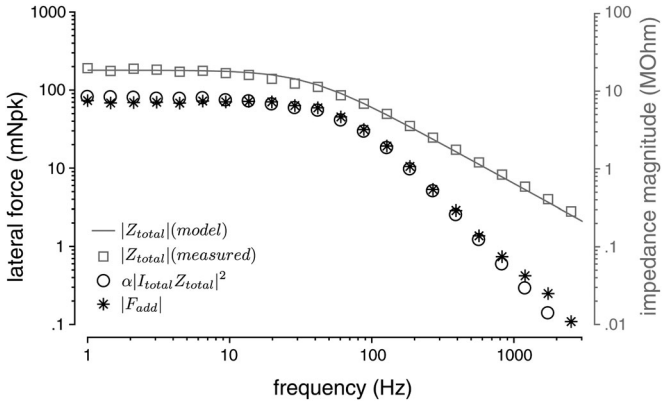

Fig. 6. Effect of the gap impedance on the force bandwidth with single sinusoid excitation (no modulation). The additional lateral force due to electroadhesion follows the same dynamic characteristic curve as the current times the gap impedance squared ($Z_{total} \approx Z_{gap}$ for 3M coating).

The first point may be neglected below our current controller's DC to 45 kHz bandwidth. The second point, however, is troublesome, as will be demonstrated by the following experiment. Note, however, that with current control the electrical dynamics of other environmental impedances, such as the impedance from the skin, or the surface coating itself, do not directly contribute to the electroadhesive force dynamics. This is a key difference between current and voltage controlled systems, as detailed in [3].

5.2 Measured Impact

The 3M coated surface affords a chance to test the force predictions made about the gap impedance, as the gap impedance is essentially the total impedance, implying $Z_{gap} \approx Z_{total}$. This means we can directly measure the dynamic parameters in Equation (8) as we are measuring F_{add} and see how they compare. This could not be done with the DLC surface, as the gap impedance is not as high a proportion of the total impedance, and as it was found the DLC surface exhibits electrical non-linearities at low frequency, which further complicate interpretation of the results.

A sinusoidal test current of $\pm 10\ \mu$A was used at individual logarithmically spaced frequencies from 1 Hz to 3,000 Hz. Applied current and voltage magnitudes were measured using a digital lock-in technique. When an electroadhesive system is subjected to single sinusoid excitation (with zero DC offset) the force response is a sinusoidal ripple at twice this excitation frequency, plus a rectified DC component. It is this double frequency ripple component of force that was recorded in this experiment, again using a digital lock-in technique.

Lateral force, therefore, was recorded from 2 Hz to 6,000 Hz in a series of 10 sequential trials (frequency order was randomized within trials). Additionally, a $10\ M\Omega$ resistor was connected from the current output to ground in order to stabilize the DC impedance of the system. This resistance bleeds off excess charge at DC, keeping the electrical system symmetric, with no appreciable DC voltage component. It was confirmed that the impact of this resistor on the system dynamics was minimal, and did not change the conclusions of the experiment.

Results of the experiment are shown in Fig. 6. This plot shows the peak lateral force magnitude, $|F_{add}|$, which occurs

at twice the frequency of the total peak current. Total impedance, Z_{total}, was also recorded and shown, along with a simple RC impedance model. An estimate of the expected lateral force was calculated from Equation (8), and is also shown (the calculation of α is discussed in the next section).

5.3 Discussion

First, we see that the gap impedance magnitude is generally flat at low frequencies and begins to attenuate at a rate of -20 dB/decade as the frequency increases. This transition takes place roughly at the RC cutoff frequency of the gap, $f_{RC} = 1/(2\pi R_{gap} C_{gap})$. The impedance could be fit well with a $R_{gap} = 17M\Omega$ in parallel with a $C_{gap} = 250$ pF, resulting in $f_{RC} = 37$ Hz (seen Fig. 6). This calculation implies that not only will the resulting voltage (and thus force) begin to attenuate at very low frequency, but that the most volatile and unknown region of the electrical system dynamics occurs in the relevant tactile frequency range of interest. To put another way, changes to the electrical dynamics far below or above the cutoff frequency are only due to R_{gap} or C_{gap} respectively. Near the cutoff frequency, however, the dynamics are influenced by both R_{gap} and C_{gap} simultaneously.

Second, Fig. 6 confirms the impact of the gap impedance dynamics on the force bandwidth, as predicted by Equation (8). This is evidenced by the fact that the estimate of the lateral force, $\alpha|I_{total} Z_{total}|^2$, and the recorded lateral force, $|F_{add}|$, share a nearly identical curve shape and magnitude, differing only by a factor of about ± 5 percent. The force attenuation due to the electrical dynamics, therefore, does not occur at a rate of -20 dB/decade, but -40 dB/decade. This means the volatile transition region between dynamic regimes happens from approximately 20-200 Hz. This is troublesome as this range is also that of peak tactile sensitivity. Since our goal was to develop a broadband excitation method with ideally flat frequency dynamics, it does not appear that the direct modulation approach is well suited for the task. Even if we were to compensate for the dynamic curve of Fig. 6 by boosting higher frequency current, for instance, there is no reason to believe that this compensation would remain valid across users or across different environmental and surface contact conditions. Instead, the rest of this paper will focus on a high frequency amplitude modulation approach to excitation, which we have found to be exceptional in its dynamic characteristics and overall performance, and which avoids this transition region.

As a final note in this section, α was calculated using μ = 0.2, ε_{gap} = 1, an average gap distance, d_{gap} of 1.1 μm (which calculated by knowing C_{gap} = 250 pF), and $A_{gap} = 30$ mm^2. The value A_{gap} is assumed to be the apparent fingerprint ridge contact area, which has been found to be an average of 30 percent of the total apparent fingerprint contact area [33]. While the estimate of α could no doubt be made better by an improved measurement of μ and A_{gap}, the insensitivity of α with frequency and its relative accuracy serve as strong empirical support for the fundamental force and impedance models hypothesized earlier. In fact, it is the opinion of the authors that no electroadhesive force model would be able to capture the behavior observed in Fig. 6 without including the air gap impedance as a central part of said model.

6 Application of Broadband Forces

6.1 Ripple versus Rectified Forces

As mentioned previously, applying single sinusoidal current or voltage excitation to an electroadhesive system yields two force components: a sinusoidal ripple force at twice the excitation frequency, and a rectified DC component. The ripple force is what was measured in Fig. 6, and what is used as the primary method of tactile excitation for many finger based electroadhesive setups such as [1], [2], [21], [22], [23], [25], [27], [28].

An alternative manner of exciting these types of systems focuses not on this ripple force, but on the rectified force component. First demonstrated Meyer et al. [24], a high frequency carrier wave can be used wherein the force component at twice the excitation waveform is simply a byproduct of the actuation, and it is the rectified DC force component that is intended to be felt as feedback by the user. In this method, the ripple component should be placed at least at a supratactile frequency ($>$1,000 Hz) and probably at a ultrasonic frequency ($>$20,000 Hz) since it can create incidental audible noise at large amplitudes. The strength of the rectified force component can then be further adjusted in time by modulating the instantaneous magnitude (envelope) of the carrier wave, as demonstrated in [14]. It is this amplitude modulated carrier approach that is expanded upon here, though now with a high performance current controller, a higher frequency carrier, different electroadhesive surfaces, and envelope magnitude shaping.

6.2 Modulation Type Used

In general, the amplitude modulation scheme used can be represented in the time domain by

$$I_{total}(t) = [1 + m(t)]^{\gamma} c(t), \quad c(t) = A_c sin(2\pi f_c t), \qquad (9)$$

where $I_{total}(t)$ is the output current of the amplifier, $m(t)$ is the desired bipolar modulation signal to be applied to the finger, and the carrier wave, $c(t)$, has amplitude A_c and frequency f_c. The parameter γ is a corrective factor used later, and for now $\gamma = 1$ simply yields double side-band full carrier (DSBFC) amplitude modulation. In this context, the instantaneous envelope of the carrier is $[1 + m(t)]$ and two limitations are placed upon the signal $m(t)$. Its frequency content must be limited to be less than f_c, and its amplitude should be small enough to ensure that the envelope always remains positive. By additionally ensuring $f_c >> f_{RC}$, we also move the electrical excitation into the purely capacitive dynamic regime and disregard any transition zone effects. One of the primary advantages to using amplitude modulation can be seen in the following experiment.

6.3 Sinusoidal Force Magnitude Response

The measured lateral force magnitude response of the 3M and DLC based electroadhesive systems using the modulation given by (9), $\gamma = 1$, is shown in Fig. 7.

Thirty logarithmically spaced modulation frequencies, 10 Hz to 10 kHz, were individually tested in a series of 10 trials. Frequency order was randomized within trials, and a 25 kHz carrier was sinusoidally modulated for 2 seconds, resulting in a 0-4 mA peak amplitude. A 4 mA maximum peak current was used to test the bandwidth of the system

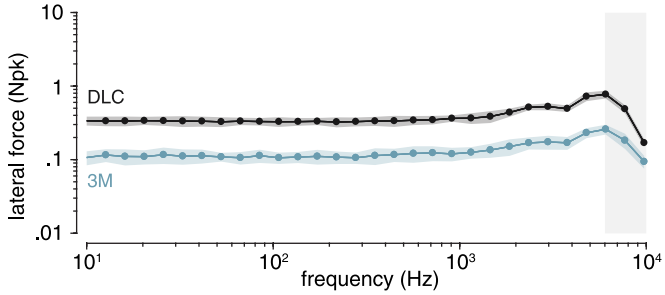

Fig. 7. Lateral force magnitude response reveals a flat response throughout entire measurement range for both the 3M and DLC based systems (recorded at 4 mApk current and 1 N normal force). Each point is the mean of 10 trials. The gray shaded region on the right denotes measurements past the resonance of the force sensing setup (included for reference, but may be ignored).

for large forces. The envelope of applied current was extracted using the analytic representation of the recorded current, found using the Hilbert transform. It was confirmed to be flat throughout this range. Lateral force peak magnitude was computed using a digital lock-in technique. The shaded regions represent $\pm\sigma$, while the solid dots and lines represent the trial means.

As seen in Fig. 7, the force response is essentially flat throughout the entire measurement range for both the 3M and DLC coated surfaces. The peak and attenuation occurring around 6 kHz (denoted by the gray shaded region) is most likely a result of the force sensor's inherent resonance (shown in Fig. 4c) and is not believed to be reflective of the transduction process. In fact, there is little evidence or theory to suggest appreciable force attenuation above 6 kHz, as strong audio response is still recorded at higher modulation frequencies. Even greater bandwidth force measurements would be needed to test this hypothesis.

The dramatic difference between the force bandwidth observed in Figs. 6 and 7 is a main advantage to using a modulated carrier approach. This, of course, does not come without some disadvantage, as the amount of applied current must be increased (approximately 2 orders of magnitude) in order to achieve the same gap voltage at higher frequency. The amount of overall real power dissipation, however, is still low, as the applied current is almost entirely capacitive, and is not electrically dissipated. Recycling this reactive current, for instance, could be an interesting topic for further research.

Finally, note that the lock-in technique analyzes only the first harmonic of each excitation frequency. While this is the largest force component measured, it does not say anything about the amount of harmonic or intermodulation distortion present. To look at these effects, we examined the quasi-static envelope curves for each system, as well as what happens when more than one sinusoid is applied.

6.4 Quasi-Static Transduction Curves

Representative quasi-static curves of total peak current versus measured lateral force for both 3M and DLC coated systems can be seen in Fig. 8. Carrier waves were sinusoidally modulated at 10 Hz for 30 seconds, yielding 300 traces of each curve. Little hysteresis was observed, and traces were binned and averaged. The shaded regions represent $\pm\sigma$, while the solid lines represent trace means.

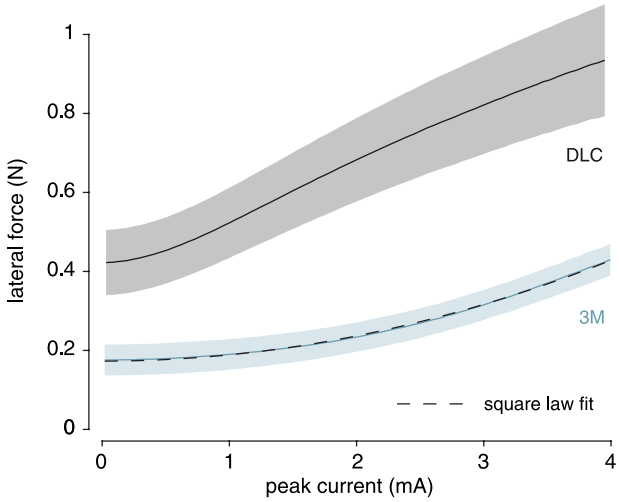

Fig. 8. Recorded lateral force (N) versus peak current (mA), averaged over 30 seconds of 10 Hz sinusoidal modulation (1 N normal force). Data was binned and averaged. The solid lines represents the trace means, and the shaded regions denotes $\pm\sigma$. An offset square law, represented by a dashed line, can be fit to curve resulting from the 3M coated surface.

The total peak current envelopes were computed as the magnitude of the analytic representation of measured current. Applied peak voltages remained below approximately 150 V, and a plot of voltage versus lateral force yielded the same shapes as Fig. 8, as the total system impedances remained essentially linear. The curves are offset due to normal kinetic friction, approximately 0.2 and 0.4 N for the 3M and DLC surfaces respectively. The additional lateral forces above these nominal friction levels are a result of the electroadhesion force, as described by Equation (6).

As can be seen in Fig. 8, the current to force transduction curve is different in both shape and dynamic range for the 3M and DLC coated surfaces. The DLC coated surface appears to have a kinetic coefficient of friction that is approximately twice that of the 3M screen, which may contribute to the fact that the dynamic range of the lateral force is also approximately twice that of the 3M screen for the same amount of peak current.

This comparison, however, is difficult to make, as the DLC exhibits a non-linear force behavior that cannot be captured by a simple power law. The force curve appears to be quadratic for low currents (<1 mApk), but it quickly begins to level off and saturate. This behavior is not predicted by our force models, but it is speculated that it could be related to the exceptionally low roughness of the surface itself ($R_{RMS} = 35$ nm). Further investigation into its origin is needed.

In contrast, the 3M coated surface (which has $R_{RMS} = 193$ nm) exhibits behavior that is consistent with a square law based transduction model. An offset square law can be fit to the data quite well, and the linear scaling coefficient from this fit is within approximately a factor of 1.5 from the scaling constant α used in Fig. 6. This is quite encouraging, as these data were taken at different times, and using different frequencies and peak current amplitudes. This suggests that the additional lateral force due to electroadhesion may be able to be approximately predicted by monitoring the electrical impedance, similar to

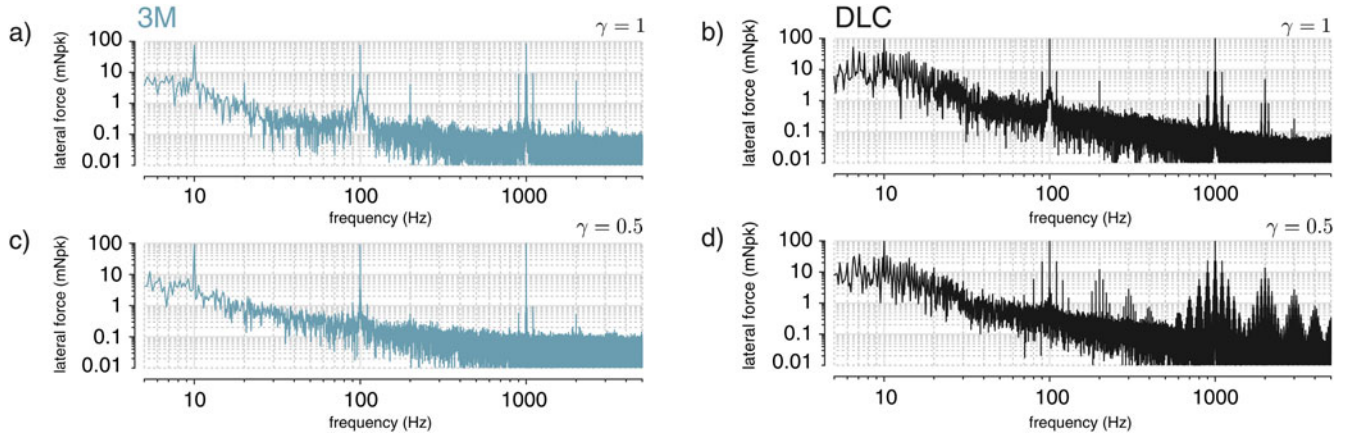

Fig. 9. Magnitude spectra of the lateral force (mNpk) recorded from 10 seconds of a multi-harmonic sinusoidal modulation excitation for both the 3M (a and c) and DLC (b and d) coated surfaces. The modulation signal contained the sum of a 10 Hz, 100 Hz, and 1,000 Hz sinusoid, each at a relative amplitude of 1/3. On the top row (a and b), the shaping parameter $\gamma = 1$, resulting in normal DSBFC amplitude modulation. On the bottom row $\gamma = 0.5$, resulting in a square rooting of the modulation envelope. Distortion products are minimal in the case of the 3M coated surface with envelope correction applied.

the method recently used in [34] with electroadhesive pucks. Further inquiry into this line of research, however, would be needed.

As a summary of Fig. 8, neither the 3M or DLC coated surfaces produce a pure sinusoidal output force given sinusoidal input modulation current; this is the very definition of the systems being non-linear. However, they do produce their first harmonic at the same frequency of the input modulation sinusoid, which is more than can be said for electroadhesive systems using a direct modulation approach. In fact, it is the addition of the DC offset to the modulation envelope (i.e., our restriction that the instantaneous envelope function remain positive) that helps avoid frequency doubling distortion. Instead, the distortion comes from the shape of the transduction curves. Because of this fact, an additional envelope shaping step may be used to reduce distortion of the system further, if desired. This is illustrated in the following section.

6.5 Envelope Shaping & Broadband Harmonic Signals

In order to further inspect the current to force distortion characteristics of the system a modulation signal consisting of the sum of 10, 100, and 1,000 Hz sinusoids was used and the resulting force was measured. Each sinusoid had a relative amplitude of 1/3 in order for the overall envelope to be close to fully modulated, but non-negative. This signal was chosen as a type of worst case distortion scenario.

The two surfaces and two values of the envelope shaping parameter γ were used. The peak carrier current amplitude was approximately 4 mA, and the carrier frequency was 25 kHz. Trials were 10 seconds long, and the magnitude of the discrete Fourier transform of the resulting lateral force signals are shown in Fig. 9. The $1/f$ shaped noise floor is assumed to come from non-electroadhesive phenomenon, and thus does not contain meaningful information here. The harmonic peaks above the noise are the components of interest.

For Fig. 9a and 9b $\gamma = 1$, resulting in typical DSBFC modulation as used in Figs. 7 and 8. Here we can clearly see the effect of the non-linear current-to-force transduction, as there is not only the intended harmonics at 10, 100, and 1,000 Hz, but second harmonics at 20, 200, and 2,000 Hz, and intermodulation products at intermediate frequencies such as 100±10 Hz, 1,000±100 Hz, etc. In each case, the intended harmonics occur with approximately the same amplitude (as predicted by Fig. 7). The next largest frequency components are due to intermodulation distortion, approximately an order of magnitude down from the intended forces. At an even lower amplitude are the second harmonic distortion components, and, for the case of the DLC coating, even a third harmonic of the 1,000 Hz component can be seen above the noise.

It remains to be seen whether this level of distortion is acceptable, or even perceptible, in tactile applications. It is, however, perceptible in audio applications. Because of this, we chose to additionally test our surfaces with $\gamma = 0.5$, preemptively shaping the modulation envelope using the square root function, which should then be inverted by the transduction process. The results of Fig. 8 predict that this envelope shape should work well for the 3M coated surface, which closely matches a square law, but not at all for the DLC coated surface, which has a transduction curve that is not easily modeled.

As seen in Fig. 9c, the square rooting of the modulation envelope had a dramatic effect on the distortion components, reducing all of them by an additional order of magnitude as compared to the $\gamma = 1$ case. Here we were able to reproduce this three harmonic signal with distortions in desired force around 1 percent. This type of DSBFC modulation with a shaped envelope appears to be a relatively simple way to achieve low-distortion and surprisingly linear behavior out of what is inherently a non-linear system.

Care must be taken, however, as the envelope shaping relies exclusively on knowing the correct inverting function. As can be seen in Fig. 9d, when a square root envelope was used with a system which does not obey a square law, the DLC coated surface, the resulting force spectrum was dramatically worse than the $\gamma = 1$ case. Efforts may be made to model a different inverting function for this system, but it is not clear at this time if this behavior could be captured by a single stable function.

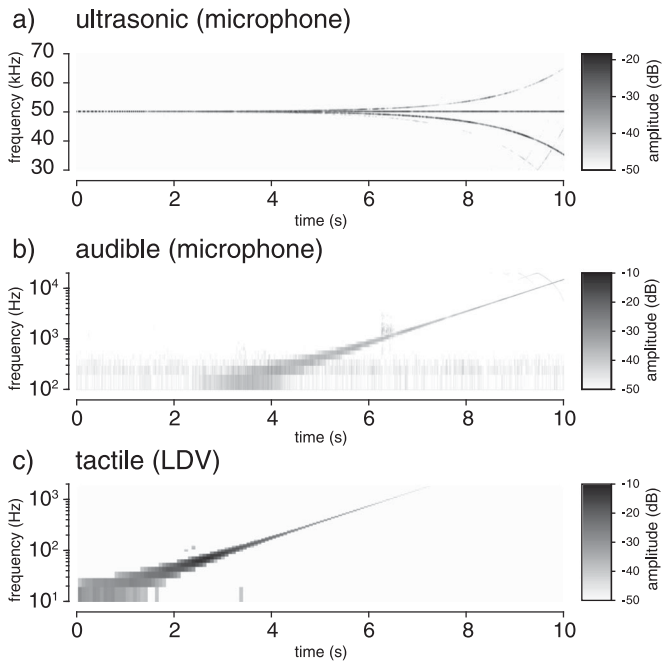

Fig. 10. Spectrogram plots of vibrations on the skin and in the air resulting from 10s logarithmic chirp current modulation (10-15,000 Hz, $f_c = 25$ kHz, $\gamma = 0.5$). a) Ultrasonic vibrations in the air are recorded as a by-product of the modulation process. b) Audible vibrations are heard and recorded emanating from the fingertip. c) Tactile vibrations are felt and recorded with the LDV.

7 Resulting Tactile, Audible, and Ultrasonic Vibrations

Thus far in our analysis we have restricted our mechanical measurements to the forces applied to the skin of the fingertip, as measured by the force ring and piezoelectric sensor. The manner in which this sensor is applied, however, effectively shunts the relatively low lateral impedance of the fingertip with the much higher impedance of the sensor, largely impeding vibration from developing and traveling up the finger. This is, of course, not how these surfaces are to be used in application, but only a useful tool for validation.

Now that we have verified a technique to apply low distortion and flat force profiles to the finger, we can release the finger from the force ring and observe vibrations as they would develop naturally. This gives us a powerful tool for probing the unhindered dynamics of a finger sliding on a flat surface. To sense these vibrations we use two non-contact methods: a MEMS microphone to capture vibrations in the air, and a laser Doppler vibrometer (LDV) to record vibrations on and of the finger. The details of these instruments are given in Section 3, and the setup used for the following measurement is shown in Fig. 5.

To illustrate the extremely wide bandwidth capabilities of this modulation technique and hardware, a 10 second logarithmic chirp modulation signal was applied to the finger. Its instantaneous frequency varied continuously from 10 Hz to 15,000 Hz. This modulation signal was applied to the 3M coated surface with $\gamma = 0.5$, a carrier frequency of 25 kHz, and a peak carrier amplitude of 4 mA. A 1 MΩ resistor was placed from the output of the amplifier to ground, once again to stabilize the DC impedance of the 3M screen. This resistor has minimal effect on the electrical system at 25 kHz, but ensures no charge build-up occurs on the plate at DC.

The data recorded is shown in Fig. 10 in the form of spectrograms, with different plots broken up into tactile, audible, and ultrasonic frequency ranges. The MEMS microphone was used for Fig. 10a and 10b, while the LDV response is shown in Fig. 10c. The plots were created using a Hanning window function and 25 percent window overlap. Window lengths of 5 ms, 10 ms, and 100 ms were used for the ultrasonic, audible, and tactile ranges respectively since the short time Fourier transform does not scale window length with frequency. Microphone and LDV response amplitudes were normalized by their peak value and the were thresholded at -50 dB.

Beginning at 0 seconds, the chirp signal's instantaneous frequency is 10 Hz, and we can see this produces a rectified vibration of the fingertip at that frequency. Also note the immediate response of the microphone at 50 kHz, twice the carrier frequency. This is the first direct evidence of ultrasonic ripple forces being applied to the skin using electroadhesion. As time progresses and the chirp's frequency increases, we see the single rectified harmonic vibration of the finger also increase. At approximately 3 seconds, the chirp is at about 100 Hz, and we start to pick up the rectified vibration in the air as well. The vibration on the skin increases further in frequency until approximately 1 kHz (and 6 seconds), where it then attenuates below the -50 dB threshold. The microphone audible response, however, continues to increase. Looking at the ultrasonic ripple response, we can also start to see the upper and lower sidebands now clearly diverging from the center frequency as the modulation frequency becomes large with respect to the carrier. Finally, we see the audible and ultrasonic response continue all the way to the end of the chirp at 10 seconds. At this point there are 4 harmonics picked up by the microphone, at 15, 35, 50, and 65 kHz.

In this example we used an instantaneously narrowband signal in order to visualize how vibrations can be induced across an exceedingly large range of tactile, audible, and ultrasonic frequencies, with small amounts of harmonic distortion. With this modulation technique and hardware in place, however, it should be appreciated that there is little hindering the excitation of the entire frequency spectrum at once with broadband force signals, as demonstrated by Fig. 9. Thus, our primary research goal of developing a system which offers broadband and rich excitation of rapidly adapting tactile afferents is achieved.

8 Conclusion & Future Work

The recordings and models reported here have several implications for surface haptic and audio-haptic displays. To begin, this current controlled, high frequency modulation technique can be readily applied to the entire frequency range of perceivable tactile forces (DC-1 kHz). As shown by Fig. 9, broadband force spectra can be easily applied to the finger, and envelope magnitude shaping may be employed to reduce harmonic and intermodulation distortion to levels seemingly on par with frictional noise. Therefore, we verify the assumption of previous research that electroadhesive based devices are well suited for high bandwidth tactile force rendering.

Additionally, our analysis reinforces the point that high performance hardware is needed if high performance, safe, and repeatable results are to be expected. For example, even

if only a 1 kHz force bandwidth is desired, at least a 11 kHz carrier should be used so that the ripple forces don't leak into the audible frequency range and distract from user perception. At higher frequency, however, greater currents are needed to generate the same air gap voltage and force, which increases the risk of inadvertent electrocutaneous stimulation. The use of current control dramatically reduces this risk.

In the case of audio-tactile displays, initial measurements such as Fig. 10 show promising results. The frequency range of resulting vibrations is exceedingly large, and signals such as intelligible speech and musical song are able to be produced by the finger while remaining remarkably recognizable to the human ear. Achieving this fidelity, however, demands still higher performance hardware ($f_c > 20$ kHz).

Further research into the current-to-audio transfer function characteristics should also be performed. Early microphone measurements in the acoustic near field suggest the resulting audio response may be relatively flat, but factors influencing the propagation of electroadhesive induced sound away from the fingertip have yet to be revealed. The impact of the acoustic properties of the contacting surface have also yet to be investigated.

As far as ultrasonic implications, it appears that the friction switching capabilities of electroadhesion, recently demonstrated by Mullenbach et al. [35], could possibly extend into the ultrasonic regime, as there appears to be considerable friction modulation capability at frequencies of 50 kHz and higher. This could lead to audibly silent active forcing of the finger, which would expand the practical capabilities of surface haptic devices in an intriguing new direction.

Finally, the insights given by the air gap impedance based force model and discussion of section 5 not only led to the experiments and conclusions above, but offer up a research direction for electroadhesive friction modulation focused squarely on the design and optimization of the skin/surface interface and resulting air gap. Questions that remain to be answered include: How might the charge accumulation or intensity of the electric field in the gap be maximized? How can the surface geometry and material optimize the amount of friction force for the same applied electroadhesive normal force? What limits the amount of applied gap voltage, or what might lead to its collapse or degradation? Answers to these questions would not only lead to better surface haptic displays, but would also yield to a better understanding of the physics behind the 140 years of electroadhesive observations.

Acknowledgments

This material is based upon work supported by the National Science Foundation grant number IIS-1518602. This work utilized Northwestern University Micro/Nano Fabrication Facility (NUFAB), which is partially supported by Soft and Hybrid Nanotechnology Experimental (SHyNE) Resource (NSF ECCS-1542205), the Materials Research Science and Engineering Center (DMR-1720139), the State of Illinois, and Northwestern University. Thanks to Oerlikon Balzers Coating USA, Inc. for the DLC coating, and Philip Chehade for processing the 3M discs.

References

[1] J. Linjama and V. Mäkinen, "E-Sense screen: Novel haptic display with capacitive ElecTrosensory interface," *HAID*, vol. 9, pp. 10–11, 2009.

[2] O. Bau, I. Poupyrev, A. Israr, and C. Harrison, "TeslaTouch: Electrovibration for touch surfaces," in *Proc. 23nd Annu. ACM Symp. User Interface Softw. Technol.*, 2010, pp. 283–292.

[3] C. Shultz, M. Peshkin, and J. Colgate, "Surface haptics via electroadhesion: Expanding electrovibration with Johnsen and Rahbek," in *Proc. IEEE World Haptics Conf.*, Jun. 2015, pp. 57–62.

[4] L. Winfield, J. Glassmire, J. E. Colgate, and M. Peshkin, "T-PaD: Tactile pattern display through variable friction reduction," in *Proc. 2nd Joint EuroHaptics Conf. Symp. Haptic Interfaces Virtual Environ. Teleoperator Syst. World Haptics*, Mar. 2007, pp. 421–426.

[5] M. Biet, F. Giraud, and B. Lemaire-Semail, "Squeeze film effect for the design of an ultrasonic tactile plate," *IEEE Trans. Ultrason., Ferroelectr., Freq. Control*, vol. 54, no. 12, pp. 2678–2688, Dec. 2007.

[6] E. Vezzoli, W. B. Messaoud, M. Amberg, F. Giraud, B. Lemaire-Semail, and M. A. Bueno, "Physical and perceptual independence of ultrasonic vibration and electrovibration for friction modulation," *IEEE Trans. Haptics*, vol. 8, no. 2, pp. 235–239, Apr. 2015.

[7] R. S. Johansson and J. R. Flanagan, "Coding and use of tactile signals from the fingertips in object manipulation tasks," *Nature Rev. Neurosci*, vol. 10, no. 5, pp. 345–359, May 2009.

[8] H. P. Saal, X. Wang, and S. J. Bensmaia, "Importance of spike timing in touch: An analogy with hearing?" *Current Opinion Neurobiology*, vol. 40, pp. 142–149, Oct. 2016.

[9] A. I. Weber, et al., "Spatial and temporal codes mediate the tactile perception of natural textures," in *Proc. Nat. Acad. Sci. USA*, vol. 110, no. 42, Oct. 2013, pp. 17 107–17 112.

[10] D. J. Meyer, M. A. Peshkin, and J. E. Colgate, "Tactile paintbrush: A procedural method for generating spatial haptic texture," in *Proc. IEEE Haptics Symp.*, Apr. 2016, pp. 259–264.

[11] L. R. Manfredi, et al., "Natural scenes in tactile texture," *J. Neurophysiology*, vol. 111, no. 9, pp. 1792–1802, May 2014.

[12] E. L. Mackevicius, M. D. Best, H. P. Saal, and S. J. Bensmaia, "Millisecond precision spike timing shapes tactile perception," *J. Neuroscience: Official J. Soc. Neurosci.*, vol. 32, no. 44, pp. 15 309–15 317, Oct. 2012.

[13] M. A. Harvey, H. P. Saal, J. F. D. Iii, and S. J. Bensmaia, "Multiplexing stimulus information through rate and temporal codes in primate somatosensory cortex," *PLOS Biol.*, vol. 11, no. 5, May 2013, Art. no. e1001558.

[14] D. J. Meyer, M. Wiertlewski, M. Peshkin, and J. Colgate, "Dynamics of ultrasonic and electrostatic friction modulation for rendering texture on haptic surfaces," in *Proc. IEEE Haptics Symp.*, Feb. 2014, pp. 63–67.

[15] M. Wiertlewski, D. Leonardis, D. J. Meyer, M. A. Peshkin, and J. E. Colgate, "A high-fidelity surface-haptic device for texture rendering on bare finger," in *Haptics: Neuroscience, Devices, Modeling, and Applications*. Berlin, Germany: Springer, Jun. 2014, pp. 241–248, doi: 10.1007/978–3-662-44196-1_30.

[16] M. Wiertlewski and J. E. Colgate, "Power optimization of ultrasonic friction-Modulation tactile interfaces," *IEEE Trans. Haptics*, vol. 8, no. 1, pp. 43–53, Jan.-Mar. 2015.

[17] A. Johnsen and K. Rahbek, "A physical phenomenon and its applications to telegraphy, telephony, etc," *J. Inst. Elect. Eng.*, vol. 61, no. 320, pp. 713–725, Jul. 1923.

[18] G. B. Prescott, *The Speaking Telephone, Talking Phonograph, and Other Novelties*. New York, NY, USA: D. Appleton & Company, 1878.

[19] E. Gray, "Improvement in electric telegraphs for transmitting musical, tones," U.S. Patent US166 096 A, Jul., 1875, cooperative Classification H04L27/26.

[20] E. Mallinckrodt, A. L. Hughes, and W. Sleator, "Perception by the skin of electrically induced vibrations," *Sci.*, vol. 118, no. 3062, pp. 277–278, 1953.

[21] R. M. Strong and D. E. Troxel, "An electrotactile display," *IEEE Trans. Man-Mach. Syst.*, vol. 11, no. 1, pp. 72–79, Mar. 1970.

[22] S. Grimnes, "Electrovibration, cutaneous sensation of microampere current," *Acta Physiologica Scandinavica*, vol. 118, no. 1, pp. 19–25, 1983.

[23] D. J. Beebe, C. M. Hymel, K. A. Kaczmarek, and M. E. Tyler, "A polyimide-on-silicon electrostatic fingertip tactile display," in *Proc. 17th Int. Conf. Eng. Med. Biol. Soc.*, Sep. 1995, pp. 1545–1546, vol. 2.

[24] D. Meyer, M. Peshkin, and J. Colgate, "Fingertip friction modulation due to electrostatic attraction," in *Proc. World Haptics Conf.*, 2013, pp. 43–48.

[25] G. Ilkhani, M. Aziziaghdam, and E. Samur, "Data-driven texture rendering on an electrostatic tactile display," *Int. J. Human–Comput. Interaction*, vol. 33, no. 9, pp. 1–15, Jan. 2017.
[26] Y. Vardar, B. Güclü, and C. Basdogan, "Effect of waveform on tactile perception by electrovibration displayed on touch screens," *IEEE Trans. Haptics*, vol. 10, no. 4, pp. 488–499, Oct.-Dec. 2017.
[27] J. Kang, H. Kim, S. Choi, K.-D. Kim, and J. Ryu, "Investigation on low voltage operation of electrovibration display," *IEEE Trans. Haptics*, vol. 10, no. 3, pp. 371–381, Jul.-Sep. 2017.
[28] H. Zophoniasson, C. Bolzmacher, M. Anastassova, and M. Hafez, "Electrovibration: Influence of the applied force on tactile perception thresholds," in *Proc. Zooming Innovation Consum. Electron. Int. Conf.*, May 2017, pp. 70–73.
[29] *IEEE Standard for Safety Levels With Respect to Human Exposure to Electromagnetic Fields, 0-3 kHz*, IEEE Std C95.6-2002, Oct. 2002.
[30] *IEEE Standard for Safety Levels with Respect to Human Exposure to Radio Frequency Electromagnetic Fields, 3* kHz *to 300* GHz, IEEE Std C95.1–2005 (Revision of IEEE Std C95.1-1991), pp. 1–238, Apr. 2006.
[31] G. King, "Bootstrapping your op amp yields wide voltage swings," 1999. [Online]. Available: https://www.edn.com/design/analog/4361336/Bootstrapping-your-op-amp-yie lds-wide-voltage-swings
[32] M. Wiertlewski and V. Hayward, "Mechanical behavior of the fingertip in the range of frequencies and displacements relevant to touch," *J. Biomechanics*, vol. 45, no. 11, pp. 1869–1874, Jul. 2012.
[33] T. Soneda and K. Nakano, "Investigation of vibrotactile sensation of human fingerpads by observation of contact zones," *Tribology Int.*, vol. 43, no. 1, pp. 210–217, Jan. 2010.
[34] T. Nakamura and A. Yamamoto, "Interaction force estimation on a built-in position sensor for an electrostatic visuo-haptic display," *ROBOMECH J.*, vol. 3, no. 1, Dec. 2016, Art. no. 11.
[35] J. Mullenbach, M. Peshkin, and J. E. Colgate, "eShiver: Lateral force feedback on fingertips through oscillatory motion of an electroadhesive surface," *IEEE Trans. Haptics*, vol. 10, no. 3, pp. 358–370, Jul.-Sep. 2017.

Craig Shultz received the BSc degree in electrical engineering from the University of Tulsa, and the master's and PhD degrees in mechanical engineering from Northwestern University. He has developed multiple ultrasonic variable friction human machine interfaces such as the TPad Fire, TPad Tablet, TPad Flow, and TPad Phone, and investigated the forgotten audio-tactile capabilities of the electroadhesive effect. In the classroom, he has co-developed and taught courses on product interaction design at the Segal Design Institute. He is a member of the IEEE.

Michael Peshkin is the Bette and Neison Harris professor of teaching excellence in the Department of Mechanical Engineering, Northwestern University, Evanston, Illinois. His research interests include haptics, robotics, human-machine interaction, and rehabilitation robotics. He has cofounded four start-up companies: Mako Surgical, Cobotics, HDT Robotics, and Tanvas. He is a fellow of the National Academy of Inventors, and (with J. E. Colgate) an inventor of cobots. He is a senior member of the IEEE.

J. Edward Colgate is the Breed University Design professor with Northwestern University. He is known for his work in haptics and human-robot collaboration. He served as an associate editor of the *IEEE Transactions on Robotics and Automation*, and he was the founding editor-in-chief of the *IEEE Transactions on Haptics*. He was one of the founding codirectors of the Segal Design Institute, Northwestern University. He has founded three start-up companies the most recent of which, Tanvas Inc., is commercializing an innovative haptic touch screen. He is a fellow of the IEEE and the National Academy of Inventors.